

# Structural, optical and electrical properties of $\text{Cu}_2\text{SnS}_3$ nanoparticles synthesized by simple solvothermal technique

S. Rabaoui · H. Dahman · N. Ben Mansour ·  
L. El Mir

Received: 4 July 2014 / Accepted: 10 November 2014 / Published online: 26 November 2014  
© Springer Science+Business Media New York 2014

**Abstract**  $\text{Cu}_2\text{SnS}_3$  (CTS) nanoparticles were successfully synthesized by simple solvothermal technique maintained at 200 °C for 24 h. The structural properties showed that the  $\text{Cu}_2\text{SnS}_3$  nanoparticles exhibit cubic phase with high crystallinity and a grain size between 11 and 15 nm. CTS nanoparticles exhibited a broad absorption in a wide wavelength range from UV to visible light, with a direct band gap of 1.27 eV. The electrical properties of the synthesized material show a variation of the conductivity as a function of measurement temperature. The dc sample conductivity measurements reveal that 3D-VRH is the dominated conduction model in the studied material. However, the dynamic conductivity study shows that correlated barrier hopping model may be appropriate to describe the transport mechanism in our material.

## 1 Introduction

In recent years, ternary systems Cu–Sn–S have shown strong application potential in many fields since they were discovered because of their properties, including high surface area, unusual optical and electronic properties [1–5].  $\text{Cu}_2\text{SnS}_3$  with interlayer spaces and tunnels in its crystal

structure, as well as the well-dispersed and uniform morphology, could be the potentially ideal lithium-ion battery electrode material [6]. The preparation of non-toxic semiconductor materials with controllable morphology and size is always one of the trends in materials research [7, 8]. On the other hand, the ternary compound  $\text{Cu}_2\text{SnS}_3$  has a structure similar to  $\text{Cu}_2\text{ZnSnS}_4$ , and is also considered a promising candidate for thin film solar cell absorber materials due to its suitable band gap energy (in a range of 0.9–1.3 eV dependent on different crystal structures [9–11]). The polymorphic state of a grown CTS is dependent on the growth temperature, where the cubic CTS is known to be formed at high temperatures (>800 °C) and the monoclinic and triclinic as well as the tetragonal phases are low temperature phases (<800 °C) [12, 13].

There are many methods to prepare CTS thin films and nanoparticles, such as conventional solid-state reaction, solvothermal processes, evaporation, spray pyrolysis technique and so on. Onoda et al. [12] prepared monoclinic CTS by a conventional solid-state reaction which requires elevated temperature, inert atmosphere protection and a relative long duration. Bouaziz et al. [7] have synthesized CTS thin film by solid-state reaction under vapor sulfur pressure at 530 °C for 6 h by using sequentially deposited copper and tin layers. Recently, a solvothermal technique, which was carried out at relatively low temperature and did not require organometallic or toxic precursors, was developed as a mild route to synthesize materials [14]. In a recent work, we have successfully synthesized a thin  $\text{Cu}_2\text{SnS}_3$  film using sol–gel spin coating route [15]. In contrast to conventional synthetic methods, solvothermal technique offers many advantages, including the enhancement of solubility, diffusion, and crystallization as well as the control of the morphologies, sizes and phase transformation, etc. [14, 15].

S. Rabaoui (✉) · H. Dahman · N. Ben Mansour · L. El Mir  
Laboratory of Physics of Materials and Nanomaterials Applied at Environment (LaPhyMNE), Faculty of Sciences, Gabès University, 6072 Gabès, Tunisia  
e-mail: seif.rebaoui@yahoo.fr

L. El Mir  
Department of Physics, College of Sciences, Al Imam  
Mohammad Ibn Saud Islamic University (IMSIU),  
Riyadh 11623, Saudi Arabia

In this paper we report synthesis of CTS nanopowder by solvothermal technique using N,N-Dimethylformamide as a solvent. Here we have used N,N-dimethylformamide (DMF) as solvent to obtain  $\text{Cu}_2\text{SnS}_3$  nanoparticles. Hence, DMF was selected as the solvent due its high polarity to absorb the microwave energy, high dipole moment (3.82) and high boiling point (153 °C) [16]. The structural, morphology, optical and electrical properties were studied.

## 2 Experimental procedure

### 2.1 Preparation of $\text{Cu}_2\text{SnS}_3$ nanoparticles

Copper tin sulphide nanoparticles was successfully synthesized by a simple solvothermal route. All chemicals are used without further purification. In a typical synthesis process, 10 mmol of Tin(II) chloride dehydrate ( $\text{SnCl}_2 \cdot 2\text{H}_2\text{O}$ , 98 % from Sigma Aldrich), was dissolved in 200 mL N,N-Dimethylformamide (DMF, >99 % from Sigma Aldrich), 20 mmol of copper(II) acetate Monohydrate ( $\text{C}_4\text{H}_6\text{CuO}_4 \cdot \text{H}_2\text{O}$ , >99 % from Fluka) was dissolved in 200 mL (DMF), and 30 mmol thiourea ( $\text{H}_2\text{NCSNH}_2$ , >99.0 % from Merck), was dissolved in 200 mL (DMF) separately, The mixture was loaded into a 1L autoclave and maintained at 200 °C for 24 h. After cooling to room temperature naturally, the black precipitate was collected and washed several times with distilled water and absolute alcohol to remove the by-products, and then dried under vacuum at 60 °C for 5 h.

### 2.2 Characterization

The crystalline phase of the obtained nanoparticles was characterized by means of X-ray diffraction (XRD) using a Bruker D5005 diffractometer with  $\text{CuK}\alpha$  radiation ( $\lambda = 1.5418 \text{ \AA}$ , 40 kV, 40 mA). The synthesized product was also characterized using a JEM-200CX transmission electron microscopy (TEM). The specimen for TEM analysis was prepared by putting the as-synthesized powder in EtOH and immersing it in an ultrasonic bath for 15 min, then dropping a few drops of the resulting suspension onto TEM grid. The optical properties of the material were obtained by Shimadzu UV-3101PC spectrophotometer with integrating sphere in the wavelength range from 200 to 2,400 nm. Electrical investigations of  $\text{Cu}_2\text{SnS}_3$  were carried out on circular ( $2R = 1.3 \text{ cm}$ , thickness = 0.25 cm) cold pressed nanocrystalline sample with two silver pastes on parallel faces to assure Ohmic contacts. Electrical studies in a temperature range from 80 to 320 K were carried out using a liquid nitrogen cryostat where the sample was kept under vacuum during the measurements. For ac analysis, an Agilent 4294A

impedance analyzer was used to collect impedance data over a wide frequency range. We employ a parallel mode to measure conductance  $G$  using an alternating signal with voltage amplitude of 50 mV.

## 3 Results and discussion

### 3.1 Structural properties

The Fig. 1 shows the XRD patterns of the nanoparticles synthesized by solvothermal process at 200 °C for 24 h. We can notice the appearance of seven pronounced diffraction peaks at  $2\theta = 28.43^\circ$ ,  $32.97^\circ$ ,  $47.31^\circ$ ,  $56.14^\circ$ ,  $69.23^\circ$ ,  $76.46^\circ$  and  $88.13^\circ$  which can be attributed respectively to the (111), (200), (220), (311), (400), (331) and (422) planes of  $\text{Cu}_2\text{SnS}_3$  phase. All detected peaks correspond to the cubic  $\text{Cu}_2\text{SnS}_3$  structure with lattice parameter  $a = 5.438 \text{ \AA}$  which is in agreement with the data (JCPDS Card 89-2877) and are also consistent with the values reported in the literature [17].

Nevertheless, no obvious peaks attributable to other impurities were observed, confirming that the obtained product is composed of the pure cubic  $\text{Cu}_2\text{SnS}_3$  nanoparticles. The XRD pattern shows that the product is well crystallized and rather pure. The average grain size was calculated using Scherrer's formula [18]:

$$G = \frac{0.9\lambda}{B \cos \theta_B} \quad (1)$$

Where  $\lambda$  is the X-ray wavelength (1.5418 Å),  $\theta_B$  is the maximum of the Bragg diffraction peak and  $B$  is the line-width at half maximum (in radians). After a correction for the instrumental broadening, an average value of the crystallites is found to be 11–14 nm. These results are in a good agreement with those obtained by Lin et al. [19]. It

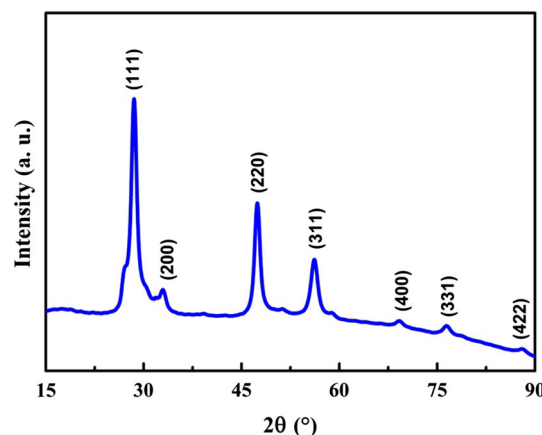


**Fig. 1** X-ray diffraction pattern of the synthesised  $\text{Cu}_2\text{SnS}_3$  nanoparticles

was found that using N,N-dimethylformamide, as a solvent, results in producing smaller nanoparticles with the cubic structures.

The Fig. 2a shows the TEM micrograph of the  $\text{Cu}_2\text{SnS}_3$  nanoparticles. The crystallites present a very similar shape with a narrow nanoparticles size distribution. The majority of these nanoparticles present in this powder have a size between 10 and 19 nm, which is comparable to that deduced from XRD spectra. The Fig. 2b shows the high resolution TEM image of  $\text{Cu}_2\text{SnS}_3$  nanoparticles taken from a portion of Fig. 2a. The lattice spacing of 0.31 nm calculated from Fig. 2b represents the (111) plane of  $\text{Cu}_2\text{SnS}_3$ , which confirms well crystalline nature of the prepared sample. The inset of Fig. 2b shows the selected area electron diffraction (SAED) pattern taken from Fig. 2a, which also reconfirmed the formation of  $\text{Cu}_2\text{SnS}_3$  crystallites. As it can be seen (inset Fig. 2b), the SAED pattern shows a set of rings instead of spots due to random orientation of the crystallites and exhibited only the cubic  $\text{Cu}_2\text{SnS}_3$  diffraction rings. The inter-planar spacing corresponding to the diffraction planes of the diffraction spots were calculated by measuring their radial distance from the directly transmitted (000) beam. The obtained distances were 0.31, 0.19 and 0.16 nm correspond respectively to (111), (220) and (311) planes related to the cubic  $\text{Cu}_2\text{SnS}_3$  phase.

### 3.2 Optical properties

The absorption spectra of the  $\text{Cu}_2\text{SnS}_3$  nanoparticles in the UV–visible–NIR range are presented in Fig. 3a. The absorption curve exhibits an intensive absorption in the range 200–380 nm, with the absorption edge between 220 and 270 nm, owing to the relatively large exciton binding energy, these findings are agrees well with those obtained by Liang et al. [17]. The optical energy band gap ‘ $E_g$ ’ is

determined using the following relation, which is valid for direct band gap semiconductors [20].

$$(\alpha h\nu)^2 = A(h\nu - E_g) \quad (2)$$

Where  $\alpha$  is the absorption coefficient,  $h\nu$  is the photon energy and  $E_g$  is the band gap energy. From Eq. (2), a Tauc plot can be drawn of  $(\alpha h\nu)^2$  versus  $h\nu$ . The point of the extrapolation of the linear part that meets the abscissa will give the value of the band gap energy ( $E_g$ ) of the material. The Fig. 3b shows the Tauc plot of the  $\text{Cu}_2\text{SnS}_3$  material. The obtained value of the  $\text{Cu}_2\text{SnS}_3$  nanoparticles band gap energy is about 1.27 eV. These results are in good accordance with the findings of Liang et al. [17] and is close to the optimum for photovoltaic solar conversion [21–23]. The near optimum band gap coupled with high absorption coefficient make CTS a potential absorber material for thin film solar cells [1, 23].

### 3.3 Electrical properties

The dc I(V) characteristic of the sample at room temperature shown in Fig. 4 outlines the ohmic behavior of the used sample. The variation of the sample conductivity versus measurement temperature  $T^{-1/4}$  in semi- log scale is shown in Fig. 5. The observed linearity indicates that the 3D-VRH mechanism may be appropriate to describe the temperature dependence of the material conductivity [24]. The VRH description is considered as equally applicable to charge carriers as electrons, holes, polarons or bipolarons provided that the suitable wave function is employed. In this model, when the interaction between charge carriers is neglected, the dc conductivity is given by:

$$\sigma_{dc} = \sigma_0 \exp\left(-\frac{T_0}{T}\right)^{1/4} \quad (3)$$

where  $\sigma_0$  is a pre-exponential factor and  $T_0$  is the characteristic temperature which determines the hopping thermal activation.

**Fig. 2** a Typical TEM of  $\text{Cu}_2\text{SnS}_3$  nanoparticles synthesized by simple solvothermal technique and b HRTEM micrograph. The inset b SAED pattern of the nanoparticles indexed to cubic  $\text{Cu}_2\text{SnS}_3$

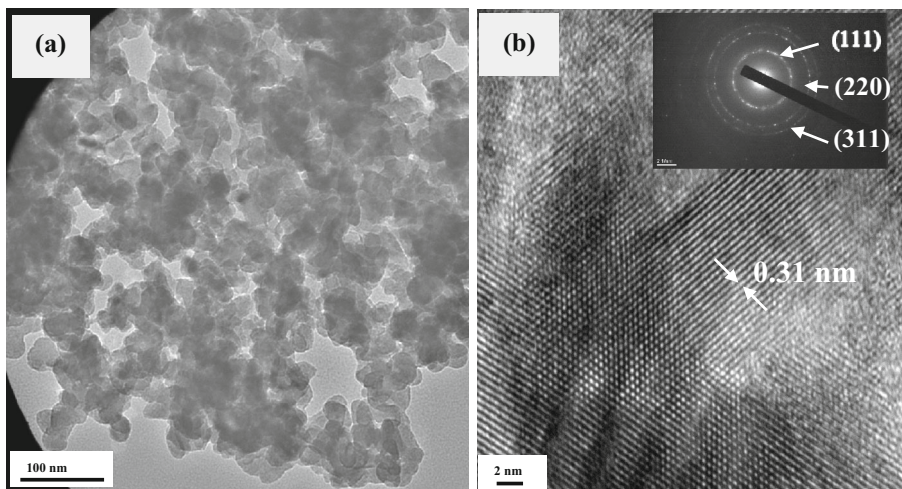


**Fig. 3** **a** Absorbance spectrum. **b** Tauc plot of  $(\alpha hv)^2$  versus  $hv$ , of the  $Cu_2SnS_3$  product

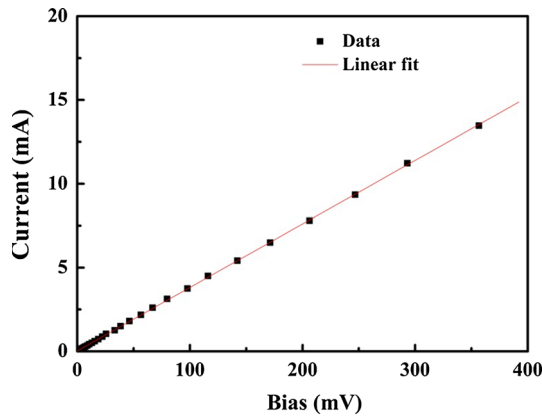
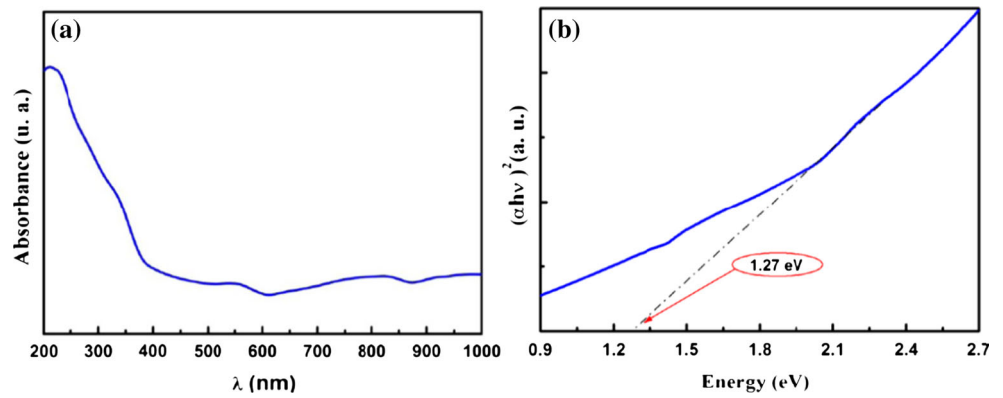


**Fig. 4** Room temperature I(V) characteristic of the  $Cu_2SnS_3$  sample

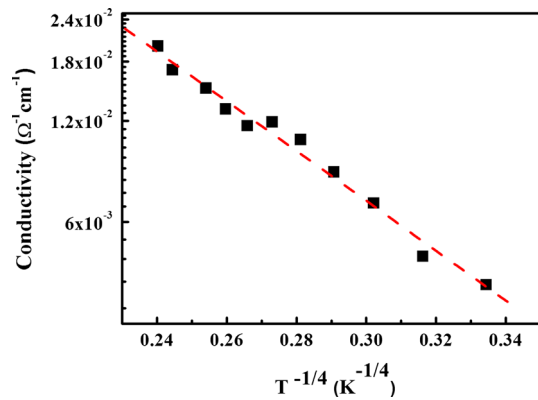


**Fig. 5** Dc conductivity versus  $T^{-1/4}$  of the used sample

In the conventional VRH model the parameters  $\sigma_0$  and  $T_0$  are functions of localization length and density of states. There is an extensive literature [25–27] on the pre-exponential factor  $\sigma_0$ . This parameter depends on the assumptions made about the electron–phonon interaction [21], and in most of cases, is considered as constant although is slightly affected by the temperature. The Fig. 6 shows the frequency dependence of the sample ac conductivity at

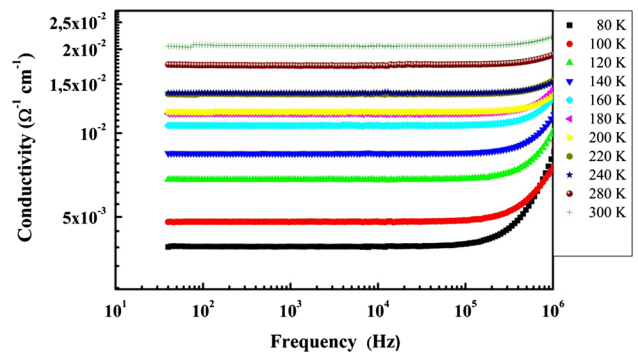


**Fig. 6** Ac conductivity versus frequency for various measurement temperatures, of the prepared material

different measurement temperatures in the log–log scale. For the full range of frequency, the material exhibits a semiconductor behavior. The characteristic features of these spectra are a plateau at low frequency region which reflects the dc conductivity regime of the material and a dispersive region at high frequency where the conductivity can be approximately described by the Jonscher’s power law [28] illustrated as follows:

$$\sigma(\omega) \propto A\omega^s \tag{4}$$

where  $A$  is a pre-exponential factor and  $s$  is the frequency exponent which may depends on temperature and frequency.

The deduced  $s$  values from fits using Eq. (4), in the high frequency region, for different measurement temperatures, are depicted in Fig. 7. The obtained values indicate that  $0 < s < 1$  characterizing the probably dominance of hopping conduction mechanism [27, 28]. The Eq. (4) is often called “the ac universality law” since it has been found to satisfactorily describe the ac response of numerous different types of materials, which can be classified as disordered.

solids [29, 30], such as ion conducting glasses [31, 32], conducting polymers [33] and polymer matrix–conductive filler composites [34]. Several theoretical models have



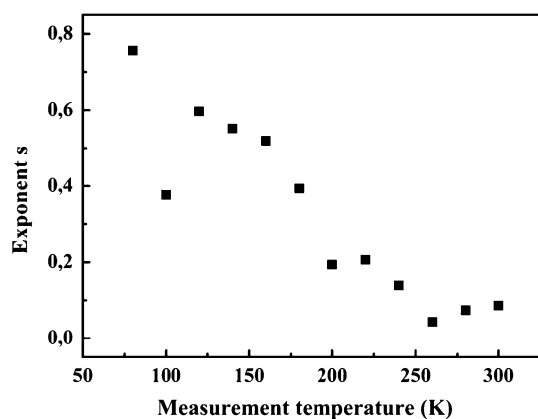


**Fig. 7** Exponent  $s$  versus measurement temperature of the synthesized  $\text{Cu}_2\text{SnS}_3$  nanoparticles

been developed to explain the frequency and temperature dependence of ac conduction in materials, such as Quantum Mechanical Tunneling (QMT) and Correlated barrier hopping (CBH) [35–37].

Experimental  $s$  values (Fig. 7) start from 0.76 and decrease and shows almost temperature independent behavior at higher temperatures, in contrast to the behavior expected for QMT [38]. In fact and according to the Eq. (5), it predicts a temperature-independent behavior.

$$s = 1 - 4/(\ln(1/\omega\tau_0)) \quad (5)$$

where  $\omega$  is the electric field frequency and  $\tau_0$  is a characteristic relaxation time (of the order of the inverse phonon frequency). In the correlated barrier hopping the exponent  $s$  can be expressed as follows:

$$s = 1 - 6kT/(W_m - kT\ln(1/\omega\tau_0)) \quad (6)$$

where  $W_m$  is the maximum barrier height of the energy band and  $k$  is the Boltzmann constant. The correlated barrier hopping predicts a decrease in  $s$  with increasing temperature, which indicates the thermally activated behavior of electron transfer over the barrier between two sites having their own Coulombic potential wells. Thus the CBH model might be a possible contending theory for ac conductivity of the present synthesized nanoparticles.

#### 4 Conclusion

In summary, nanoparticles of the ternary  $\text{Cu}_2\text{SnS}_3$  were successfully synthesized by a simple solvothermal technique maintained at 200 °C for 24 h using N, N-Dimethylformamide as solvent. The X-ray diffraction and TEM of  $\text{Cu}_2\text{SnS}_3$  nanoparticles show a crystalline cubic phase with a particles sizes ranging between 11 and 15 nm. From optical investigations, the  $\text{Cu}_2\text{SnS}_3$  nanoparticles exhibited a broad absorption in a wide wavelength range from UV to

visible light, with a direct band gap of 1.27 eV. The dc conductivity measurements of our material outline a linearity behavior in semi-logarithmic scale depending on  $T^{-1/4}$  and indicating that transport mechanism could happen within VRH model. The ac conductivity measurements of the studied sample are found to be temperature and frequency dependent and obey to the universal power law. The CBH model seems to explain the exponent  $s$  behavior while the QMT model fails to predict the temperature dependence of the frequency exponent. Structural, morphological, optical and electrical properties of the optimized sample have been investigated. The obtained results show that this is a promising starting point for future investigations of  $\text{Cu}_2\text{SnS}_3$  non toxic thin film instead of  $\text{CuInS}_2$  and  $\text{Cu}_2\text{ZnSnS}_4$ , classical materials in the fabrication of high performance photovoltaic devices.

**Acknowledgments** The authors gratefully acknowledge K. Omri for kindly providing support for the absorption and XRD analysis.

#### References

1. D. Tiwari, T.K. Chaudhuri, T. Shripathi, U. Deshpande, R. Rawat, *Sol. Energy Mater. Sol. Cells* **113**, 165–170 (2013)
2. X.-a Chen, H. Wada, A. Sato, M. Mieno, *J. Sol. State Chem.* **139**, 144–151 (1998)
3. C. Wu, Z. Hu, C. Wang, H. Sheng, J. Yang, Y. Xie, *Appl. Phys. Lett.* **91**, 143104–143106 (2007)
4. Y. Tan, Z. Lin, W. Ren, W. Long, Y. Wang, X. Ouyang, *Mater. Lett.* **89**, 240–242 (2012)
5. D.M. Berg, R. Djemour, L. Gutay, G. Zoppi, S. Siebentritt, P.J. Dale, *Thin Sol. Films* **520**, 6291–6294 (2012)
6. B.H. Qu, M. Zhang, D. Lei, Y.P. Zeng, Y.J. Chen, *Nanoscale* **3**, 3646–3651 (2011)
7. M. Bouaziz, J. Ouerfelli, S.K. Srivastava, J.C. Bernde, M. Amlouk, *Vacuum* **85**, 783–786 (2011)
8. M. Bouaziz, M. Amlouk, S. Belgacem, *Thin Sol. Films* **517**, 2527–2530 (2009)
9. D. Avellaneda, M.T.S. Nair, P.K. Nair, *J. Electrochem. Soc.* **157**, 346 (2010)
10. P.A. Fernandes, P.M.P. Salomé, A.F. da Cunha, *Phys. Status Solidi. C* **7**, 901 (2010)
11. Y. Zhai, S. Chen, J. Yang, H. Xiang, X. Gong, A. Walsh, J. Kang, S. Wei, *Phys. Rev. B* **84**, 075213 (2011)
12. M. Onoda, X.A. Chen, A. Sato, H. Wada, *Mater. Res. Bull.* **35**, 1563–1570 (2000)
13. D.M. Berg, R. Djemour, L. Gütay, S. Siebentritt, P.J. Dale, X. Fontane, V. Izquierdo-Roca, A. Perez-Rodriguez, *Appl. Phys. Lett.* **100**, 192103-1–192103-4 (2012)
14. G. Demazeau, *J. Mater. Chem.* **9**, 15–18 (1999)
15. H. Dahman, S. Rabaoui, A. Alyamani, L. El Mir, *Vacuum* **101**, 208–211 (2014)
16. R. Lotfi Orimi, N. Shahtahmasebi, N. Tajabor, A. Kompany, *Physica E* **40**, 2894 (2008)
17. X. Liang, Q. Cail, W. Xiang, Z. Chen, J. Zhong, Y. Wang, M. Shao, Z. Li, *J. Mater. Sci. Technol.* **29**, 231–236 (2013)
18. H. Saeki, H. Tabata, T. Kawai, *Sol. State Commun.* **120**, 439–443 (2001)
19. X. Lin, J. Kavalakkatt, K. Kornhuber, S. Levchenko, M.Ch. Lux-Steiner, A. Ennaoui, *Thin Sol. Films* **535**, 10–13 (2013)

20. C.H.L. Weijtens, P.A.C. Vanloon, *Thin Sol. Films* **196**, 1–10 (1991)
21. B. Li, Y. Xie, J. Huang, Y. Qian, *J. Sol. State Chem.* **153**, 170–173 (2000)
22. A. Ennaoui, M. Lux-Steiner, A. Weber, D. Abou-Ras, I. Kötschau, H.-W. Schock, R. Schurr, A. Hölzing, S. Jost, R. Hock, *Thin Sol. Films* **517**, 2511–2514 (2009)
23. K. Tanaka, Y. Fukui, N. Moritake, H. Uchiki, *Sol. Energy Mater Sol. Cells* **95**, 838–842 (2011)
24. N.F. Mott, *Phil. Mag.* **19**, 835–852 (1969)
25. N.F. Mott, *Metal–Insulator Transitions* (Taylor & Francis, London, 1990)
26. N.F. Mott, *Conduction in Non-Crystalline Materials* (Clarendon Press, Oxford, 1987)
27. H. Bottger, U.V. Bryskin, *Hopping Conduction in Solids* (Verlag Akademie, Berlin, 1985)
28. A.K. Jonscher, *Nature* **276**, 673–679 (1977)
29. J.C. Dyre, T.B. Shroder, *Rev. Mod. Phys.* **72**, 873–892 (2000)
30. A.K. Jonscher, *Universal Relaxation Law* (Chelsea Dielectrics Press, London, 1992)
31. C.A. Angell, *Chem. Rev.* **90**, 523–542 (1990)
32. B. Roling, *Sol. State Ion* **105**, 185–193 (1998)
33. M.M. Jastrzebska, S. Jussila, H. Isotalo, *J. Mater. Sci.* **33**, 4023–4028 (1998)
34. N. Guskos, E.A. Anagnostakis, V. Likodimos, T. Bodziony, J. Typek, M. Maryniak, *J. Appl. Phys.* **97**, 024304–024310 (2005)
35. M. Pollak, T.H. Geballe, *Phys. Rev.* **122**, 1742–1753 (1961)
36. M. Pollak, G.E. Pike, *Phys. Rev. Lett.* **28**, 1449–1451 (1972)
37. S.R. Elliott, *Adv. Phys.* **36**, 135–218 (1987)
38. A.R. Long, *Adv. Phy.* **31**, 553–637 (1982)